Numerical Calculation of a Tiltrotor Aircraft Aerodynamic Stability Derivatives

D. Granata, A. Savino, A. Zanotti
Politecnico di Milano, Dipartimento di Scienze e Tecnologie Aerospaziali,
via La Masa 34, 20156, Milan, Italy

ABSTRACT

The present paper is aimed to investigate the capability of mid-fidelity aerodynamic solvers to perform a preliminary evaluation of static and dynamic stability derivatives on tiltrotor aircraft configurations during their design phase. In this work, the mid-fidelity aerodynamic solver DUST based on vortex particle method (VPM) was used to perform simulations in static and dynamic motion conditions of the Bell XV-15 tiltrotor aircraft. Static simulations allowed for the calculation of static stability derivatives, while dynamic simulations, using two different approaches applied to the time history of the load in a dynamic motion, enabled the calculation of dynamic derivatives. The entire procedure was carried out following a "breakdown" approach, with the goal of highlighting the interactions between different aircraft's components (such as wing-tail and rotor-airframe), and to provide an approach for the overall assessment of Stability & Control characteristics of the aircraft. The limited computational effort required by the mid-fidelity aerodynamic approach represents an effective trade-off in obtaining fast and accurate solutions that can be used for the preliminary design of novel rotary-wing vehicle configurations.

NOMENCLATURE

C_j = aerodynamic coefficient
C_{j0} = zero attitude aerodynamic coefficient
C_l = rolling moment coefficient
C_m = pitching moment coefficient
C_n = yawing moment coefficient
C_p = pressure coefficient
c_{ref} = reference chord
C_X = X-force coefficient
C_Y = Y-force coefficient
C_Z = Z-force coefficient
k = reduced frequency = $l\omega/V$
n_c = number of periods
p = roll rate
q = pitch rate
r = yaw rate
T = period = $2\pi/\omega$
α = angle of attack
β = angle of sideslip
θ = pitch angle
ϕ = roll angle
ψ = yaw angle
ω = angular frequency

INTRODUCTION

The design phase of an aircraft is characterized by the need to predict the static and dynamic behavior of the aircraft starting from the preliminary stage of the process. The ability to obtain reliable and robust quantitative information would be useful to avoid future redesign operations. The knowledge of stability derivatives allows in fact to create linear aerodynamic models that can be implemented during the preliminary development of aircraft control systems, and allows the computation of the modes associated with the free response (i.e. for an aircraft with traditional configuration longitudinal short period, phugoid, roll subsidance, spiral, dutch roll, etc.), as well as to predict the time history of the loads acting on the aircraft in more complex maneuvers (as done by Ferguson et Al. (Ref. 1)). Different methods were developed to predict aircraft control and stability behavior throughout history.
Experimental methods for the prediction of aerodynamic coefficients and stability derivatives essentially include wind tunnel tests and flight tests with the latter representing the most reliable and safe method to obtain the required information within a higher accuracy. However, they can only be performed at an advanced stage of design since they require the availability of a working prototype of the aircraft. Wind tunnel tests also provide a high level of accuracy, but are characterized by some drawbacks such as the difficulty to calculate appropriate corrections for dynamic tests due to the presence of the walls and of the model supporting sting that could alterate the airloads evaluation. Moreover, the experimental methods are characterized by a high cost associated to the manufacturing of a model or a prototype and the realization of a complex test rig (Figure 1) particularly for dynamic tests (Ref. 2).

Computational Methods. Semi-empirical lower-order models are the simplest models characterized by the lowest level of fidelity. These methods are based on the use of empiri-

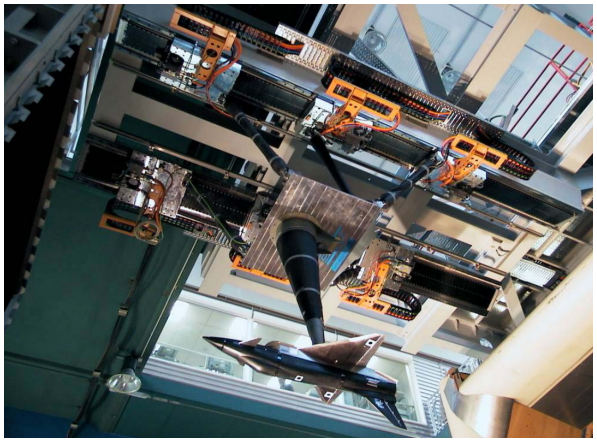

Figure 1. Realized MPM kinematic design in DNW-NWB with X-31 (Ref. 3)

cal formulas coupled with simple aerodynamic theories (such as strip theory and 2D aerodynamic theories) and allow for a direct estimation of the stability derivatives of the aircraft. Modern computational techniques provide different solutions for the appropriate estimation of stability derivatives, characterized by different levels of fidelity. These techniques include, for example, the use of high-fidelity computational fluid dynamics (CFD) or linear methods such as panel methods and vortex lattice methods (VLM). The use of computational techniques in the preliminary development of the aircraft allows to obtain a huge amount of information for different types of conditions and for different geometric configurations. However, high-fidelity CFD simulations require a huge computational effort to predict accurately the flow phenomenology, particularly considering dynamic configurations and in the case of complex configurations characterized by the presence of rotors, such as helicopters, tiltrotors, or the more modern eVTOLs (electric Vertical Take-Off and Landing vehicles), where full-machine simulations can take up to several days even with High-Performance Computing (HPC) involving thousands of processors (Ref. 4). These characteristics make it not suitable for the preliminary design stage of a novel aircraft configuration, since it requires different geometry configurations as well as different flight conditions to be tested.

In this context, the use of a mid-fidelity aerodynamic solver can be considered of fundamental importance in order to get results with a limited computational effort while keeping accuracy. Recently, Politecnico di Milano developed a novel, flexible mid-fidelity aerodynamic computational tool called DUST (Ref. 5) aimed at representing a fast and reliable asset for the simulation of the aerodynamics of complex aircraft configurations such as eVTOL aircraft and tiltrotors. DUST is an open source code, released under MIT license, integrating different aerodynamic models for solid bodies, as thick surface panels, thin vortex lattice elements and lifting lines elements. Moreover, a vortex particle method (VPM) was implemented for wake modeling providing a stable Lagrangian description of free-vorticity flow field, which is suitable for numerical simulations of configurations characterized by strong aerodynamic interactions. Details about the mathematical formulation of the solver can be found in (Ref. 5).

In the present work, results obtained with DUST are used to compute static and dynamic derivatives of the Bell XV-15 tiltrotor aircraft (Fig. 2), performing static simulations to obtain stability derivatives relative to the airframe's attitude, and dynamic simulations consisting of executing oscillatory motions to obtain dynamic stability derivatives. The results will be compared with wind tunnel experiments, analytical methods for calculating dynamic stability derivatives, and CFD (Computational Fluid Dynamics) calculations.

Figure 2. XV-15 in airplane mode

Following sections will show the methods used to calculate the stability derivatives, the numerical model of the XV-15, the choices made for simulation parameters, and the results of the simulations.

MATHEMATICAL MODEL FOR THE CALCULATION OF STABILITY DERIVATIVES

This section provides a brief summary of the methods used in the present work to compute the dynamic stability derivatives. A comprehensive overview of the methods used in this work is available in (Ref. 6), where the methodology has been validated.

The calculation of static stability derivatives is straightforward, as it only requires performing a series of static simulations by varying the angle of attack and the sideslip angle. This is done in order to derive the $C_j - \alpha$ and $C_j - \beta$ curves, whose slopes represent the static stability derivatives (C_{j_α} and C_{j_β}, respectively).

The computation of dynamic stability derivatives instead is performed by imposing a sinusoidal oscillatory motion to the aircraft in its partial or complete configuration around a material point belonging to its volume (typically the center of gravity). The definition of the main stability derivatives alongwith the aircraft motions to be considered for their calculation are briefly summarized in Tab. 1.

The hypothesis underlying the definition of stability derivatives is that forces and moments acting on the aircraft follow

Table 1. Stability derivatives and oscillatory motions

	X axis	Y axis	Z axis
Rolling	$C_{l_p}+C_{l_{\dot\beta}}\sin\alpha$	$C_{Y_p}+C_{Y_{\dot\beta}}\sin\alpha$	$C_{n_p}+C_{n_{\dot\beta}}\sin\alpha$
Pitching	$C_{X_q}+C_{X_\alpha}$	$C_{m_q}+C_{m_\alpha}$	$C_{Z_q}+C_{Z_\alpha}$
Yawing	$C_{l_r}-C_{l_{\dot\beta}}\cos\alpha$	$C_{Y_r}-C_{Y_{\dot\beta}}\cos\alpha$	$C_{n_r}-C_{n_{\dot\beta}}\cos\alpha$
Phugoid	C_{X_q}	C_{m_q}	C_{Z_q}
Lat. Phugoid	C_{l_r}	C_{Y_r}	C_{n_r}
Plunging osc.	C_{X_α}	C_{m_α}	C_{Z_α}
Lateral osc.	$C_{l_{\dot\beta}}$	$C_{Y_{\dot\beta}}$	$C_{n_{\dot\beta}}$

a linear behaviour with respect to variations of angle of attack and its derivative $\alpha,\dot\alpha$, angle of sideslip and its derivative $\beta,\dot\beta$ and angular rates and accelerations in body axes $p,q,r,\dot p,\dot q,\dot r$. Taking this hypothesis into account, it is then possible to use a first-order Taylor series development for the description of aerodynamic coefficients. As demonstrated in (Ref. 7), the aerodynamic coefficient for pitching motion can be expressed as the outcome of the Taylor series expansion as follows,

$$\Delta C_j = C_j - C_{j_0} = \alpha_A \bar C_{j_\alpha}\sin(\omega t) + \alpha_A\, k \bar C_{j_q}\cos(\omega t), \quad (1)$$

where $k = l\omega/V$ is the reduced frequency, ω is the motion frequency, V the freestream velocity, l is the reference chord for longitudinal motions and the semispan for lateral-directional motions and

$$\bar C_{j_\alpha} = (C_{j_\alpha} - k^2 C_{j_{\dot q}})\bar C_{j_q} = (C_{j_{\dot\alpha}} + C_{j_q}) \quad (2)$$

and in particular $\bar C_{j_q}$ is the dynamic "out-of-phase" stability derivative. A similar procedure can be used to obtain combined or separated dynamic derivatives for all the motions defined in Table 1. If the linear hypothesis is valid, the coefficient time history describes an hysteresis ellipse in the plane $C_j - \alpha$.

Single point method

By inverting Eq.(2) when $\omega t = 0$, it is possible to derive the out-of-phase stability derivative. This operation coincides with measuring the thickness of the hysteresis ellipse of the coefficient time history around α_0. Substituting $\omega t = 0$ in Eq.(2) yields to

$$\Delta C_j(t)\big|_{t=t_{\alpha_0}} = \alpha_A\, k \bar C_{j_q}. \quad (3)$$

Consequently, the dynamic stability derivative can be obtained as

$$\bar C_{j_q} = \frac{\Delta C_j(t)\big|_{t=t_{\alpha_0}}}{\alpha_A\, k} \quad (4)$$

Fourier coefficient method

A second method is based on considering Eq.(2) as a Fourier series truncated at the first term. Consequently, it is possible to compute the dynamic stability derivative as the Fourier coefficient of the time history of $\Delta C_j(t)$ as follows,

$$\bar C_{j_q} = \frac{2}{\alpha_A\, k\, n_c\, T}\int_0^{n_c T} \Delta C_j(t)\cos(\omega t)dt \quad (5)$$

Rolling Oscillation

In this particular subsection, the specific case of roll motion, which is used in section , is detailed. It is assumed to perform an harmonic roll maneuver, at zero angle of attack and angle of sideslip ($\alpha,\beta = 0$). The taylor series expansion of the lateral-directional aerodynamic coefficients, coupled with the kinematic law of motion, reads:

$$\begin{cases} \Delta C_j = C_j - C_{j_0} = \frac{l}{v} C_{j_p} p + (\frac{l}{v})^2 C_{j_{\dot p}}\dot p \\ \phi(t) = \phi_A \sin(\omega t), \\ \dot\phi = p = \omega\,\phi_A\cos(\omega t), \\ \ddot\phi = \dot p = -\omega^2\,\phi_A\sin(\omega t). \end{cases} \quad (6)$$

Which can be rewritten as:

$$\Delta C_j = -\phi_A\, k^2\,(C_{j_{\dot p}})\sin(\omega t) + \phi_A\, k\,(C_{j_p})\cos(\omega t) \quad (7)$$

Methods described in the previous sections can therefore be applied to Eq. (2).

XV-15 DUST NUMERICAL MODEL

This section describes the numerical model of the XV-15 which was employed in DUST. The XV-15 is a tiltrotor, an aircraft capable of rotating its nacelles to achieve three possible flight modes: helicopter mode, transition mode, and airplane mode. This work particularly focuses on the latter, the airplane mode. The geometric layout of the aircraft is depicted in figure 3(a). Figure 3(b) shows the top view of the XV-15's aerodynamic model: the main components of the aircraft are three: the wing-pylon system (modelled with surface panel elements (Ref. 5)), represented by the wing-nacelles assembly, the horizontal and vertical tail system (also modelled with surface panel elements), and the rotors (modelled with lifting line elements (Ref. 5)). In this work, the fuselage has not been modeled and will just be represented in some figures to better explain the aircraft's attitude; this decision was primarily motivated by two factors: firstly, adding the fuselage to the model would have significantly increased the computational cost for a very limited gain in the accuracy of the results. The fuselage consists of a large number of panels, and incorporating it would require additional computation time and resources. Secondly, even if the fuselage were present, the loads predicted on it by DUST would be approximate and inaccurate, as the DUST model does not account for the boundary layer and any separation that may occur due to the bluff

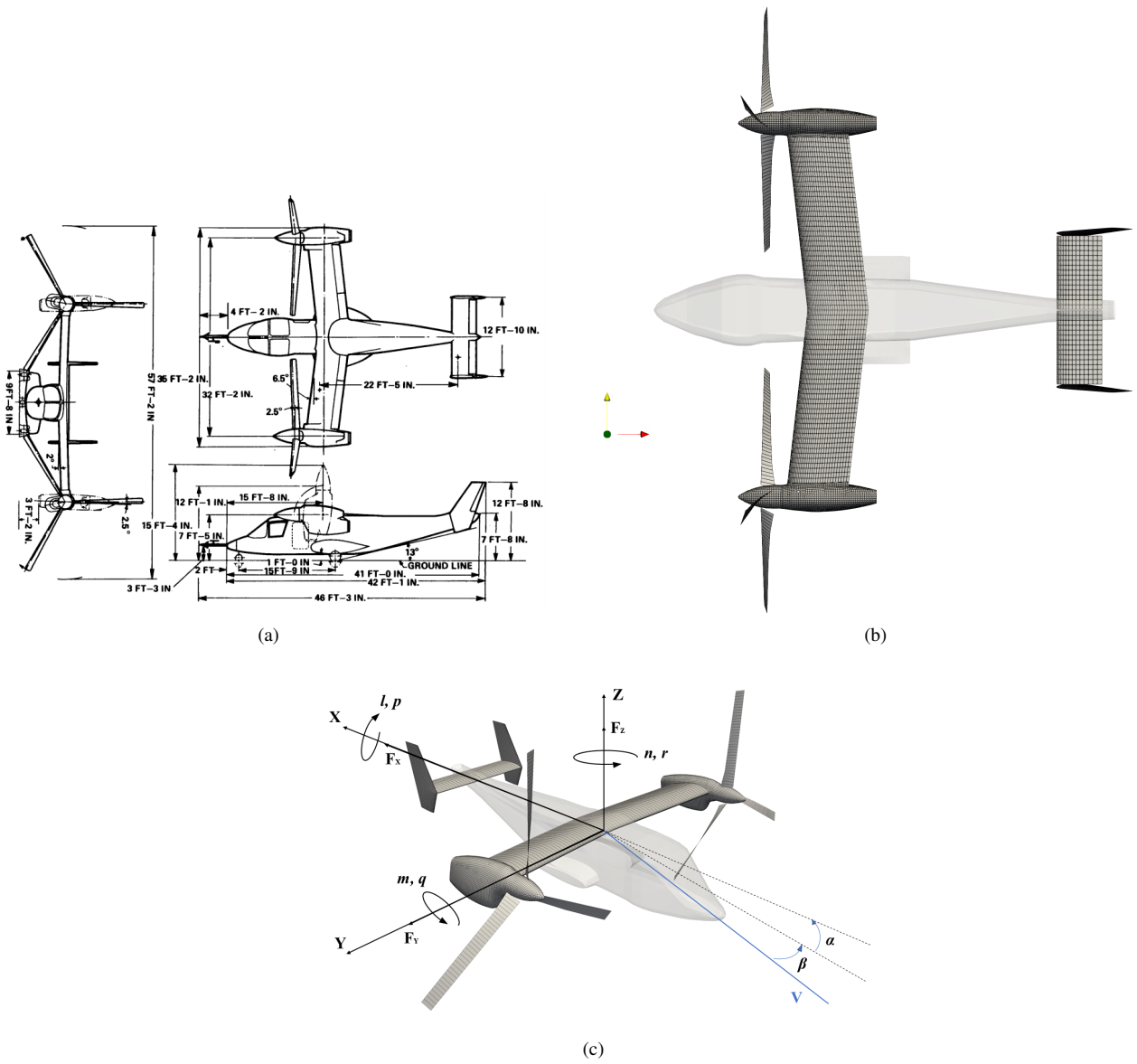

Figure 3. (a) XV-15 tiltrotor research aircraft dimensions; (b) XV-15 DUST aerodynamic mesh; (c) Definitions of the aerodynamic coefficients and reference frame.

body shape of the fuselage. Figures 3(b) and 3(c) show the mesh of the aerodynamic model, which consists of a total of 19,356 elements. The mesh was selected following a convergence study conducted in a previous work using the same model (Ref. 8). The simulation time-step is set at 0.001 seconds, which amounts to 116 time-steps per rotor revolution and 333 time-steps per dynamic oscillation of the aircraft, in the case of dynamic simulation. Figure 3(c) shows also the reference frame used in the present work to compute the aerodynamic loads: the body axes reference frame is employed with the sign convention shown in the figure 3(c). Aerodynamic coefficient were obtained by non-dimensionalizing with respect to the dynamic pressure, the main wing area, and the main wing chord and span for moments.

The work is organized with a ”breakdown” approach to the aircraft. The systems of the aircraft are analyzed both in isolated configuration and in the assembled configuration:

- *Wing-Pylon*: isolated wing and nacelles.
- *Isolated Tail*
- *Full configuration without rotors*: composed by wing-pylon, the vertical tail and the horizontal stabilizer.
- *Full configuration with rotors*: composed by wing-pylon, the vertical tail, the horizontal stabilizer and the rotors.

The breakdown approach not only allowed for the validation of the numerical model of each component thanks to available wind tunnel test data on individual components, but also for

a detailed analysis of the aerodynamic interaction effects between them, such as the wing's downwash effect on the tail, which significantly influences the loads and therefore the stability derivatives, and the rotor-airframe interaction, which results in the aircraft experiencing loads characterized by a 3/rev rotor periodicity, as well as significant stability effects on the complete machine.

Dynamic simulation with the full configuration with rotors were performed around a trimmed condition. This was made possible by adjusting manually the values of the collective blade pitch angle and the longitudinal cyclic pitch angle, which were chosen in order to match the thrust and the H-force on the rotor, as done in the work of Lim et al. (Ref. 9).

The numerical simulations were performed on a workstation made available by DAER, the Department of Aerospace Science and Technology of Politecnico di Milano. The machine has a Intel Xeon Gold 6230R processor running on a base frequency of 2.10 GHz, with 52 physical cores and 2 threads for each core. Its RAM amounts to 376 GB. For the full configuration with rotors, each static simulation took around 2 hours, while each dynamic simulation took 4 hours.

STATIC ANALYSES

In this section, static simulations results are analyzed to validate the numerical model built with DUST, to find the aerodynamic static stability derivatives of each component, and to assess interactional aerodynamic phenomena such as the downwash effect or the wing-rotor interaction. Each test point was obtained by performing a time-marching simulation of 0.333 s and the integral loads values were extracted at the end of the transient, after the solution reached a stationary condition. Static analysis involved different simulations varying the angle of attack and the angle of sideslip of the aircraft body axes frame of reference, as defined in figure 3(c). Freestream velocity for all simulations was set to 72.02 m/s, while the thermodynamic state condition were extracted with the ISA+=0 at sea level.

Wing-Pylon

In this section, the results obtained from the DUST simulations of the Wing-Pylon system, considering three different aileron deflection δ_a of 0°, 10 and 20°, are compared with the wind tunnel values shown in (Ref. 1), and with simulation performed with open source CFD software SU2 on the same configuration (Ref. 10). Figure 4(a) shows the vertical force coefficient C_Z, the longitudinal force coefficient C_X and the pitching moment coefficient as a function of the angle of attack α.

A quite good agreement with the data available in literature was found for both the computed vertical and horizontal force coefficients in body axes reference frame, as well as for the pitching moment coefficient.

Additionally, the effect of wing aileron actuation (whose implementation is explained in (Ref. 8)) is optimally captured, which indeed shows the same curve translation compared to the data provided by CFD. A slight difference is noted in the case of the C_X curve: since the parasite drag is not modeled by the mid-fidelity solver, there is a discrepancy between DUST and SU2 drag coefficient curves. On the other hand, since the induced drag generated by the wing tip vortices is almost well represented, all the curves show good coherence as a function of the angle of attack and the aileron deflection.

Figure 4(b) instead shows the stability and control derivatives extracted from the discussed graphs: static stability derivatives C_{Z_α} and C_{m_α} calculated from DUST curves are compared with Wind Tunnel and CFD values, using first-order forward differences for the derivative extraction (which is sufficient in this case given the linearity of the trend). Also in this case derivatives show excellent agreement with literature data, demonstrating the effectiveness of the numerical model built for this component. In the same way, the control derivative $C_{Z_{\delta_a}}$, which represents the aileron effectiveness, is also in good agreement.

Horizontal Stabilizer and Vertical Tail

In this section, results obtained with DUST for the isolated tail configuration, for different rudder and elevator inclinations, are compared with those obtained from wind tunnel tests, reported by Ferguson (Ref. 1). From figures 5 (a) and (b), it can be seen that, similarly to the Wing-Pylon case, the results obtained with DUST in the longitudinal static simulations are in excellent correspondence with the results of wind tunnel testing, both in terms of the body axis load curves as a function of the angle of attack, and in terms of the elevator effectiveness. At $\alpha = 15°$, with the appearance of stall, there is a divergence between the experimental data and those of DUST. The accuracy of the static curves is also seen in the values of the stability derivatives and the effectiveness of the control surface, as visible from figures 5 (c) and (d), thus validating the model constructed for the tail of the XV-15.

Figure 6 shows the tail static loads as a function of the angle of sideslip. Again, a good correspondence is found between DUST and wind tunnel data, both for the loads and for the effectiveness of the control surface. A slight discrepancy is visible on the loads of the vertical tail starting from a sideslip angle of 10°. Which is probably due to an underestimation of the lateral stability derivative visible in figure 6. It is important to emphasize that the quality of these results must also be assessed in relation to the significant gain in terms of computational resources expended compared to traditional methods of calculating stability derivatives, which were based on large experimental campaigns.

Full Configuration without Rotors

In this section, results associated with the full configuration without rotors are shown. This configuration is particularly important for quantifying the downwash effect, when compared to the isolated tail configuration.

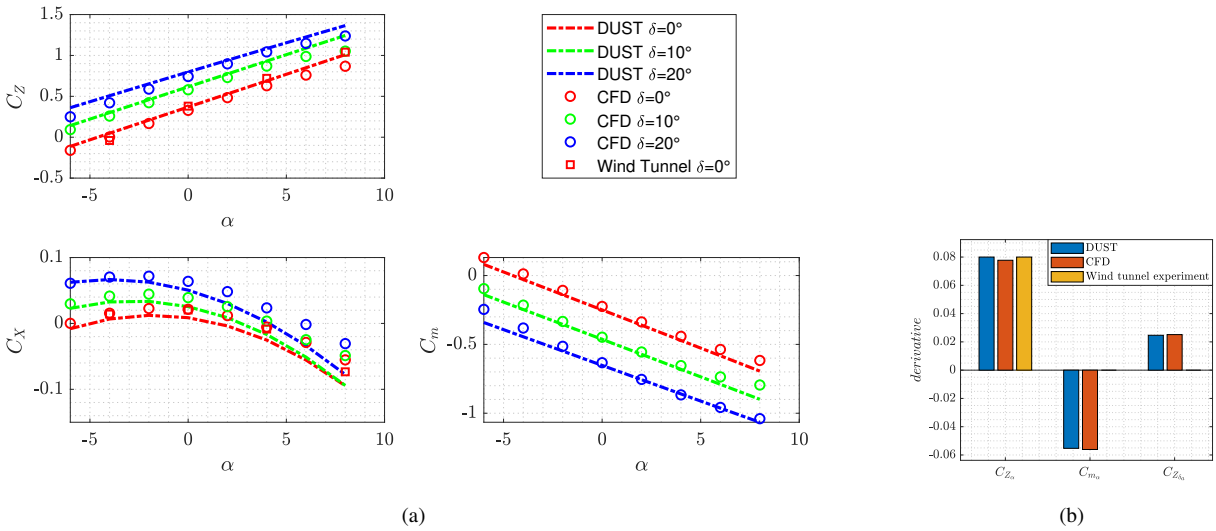

Figure 4. (a) Static curves: aerodynamic coefficients as function of the angle of attack α. Comparison with CFD SU2 and Wind Tunnel Experiment (Ref. 1). (b) XV-15 Static stability derivatives. Comparison with CFD SU2 (Ref. 10) and Wind Tunnel Experiment (Ref. 1)

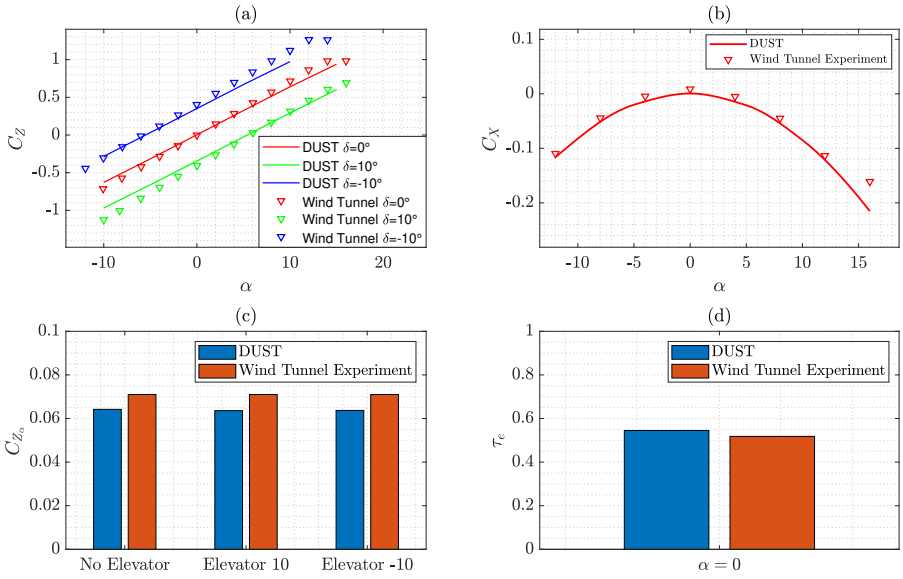

Figure 5. Isolated tail static loads: aerodynamic coefficients as function of the angle of attack; Longitudinal stability derivatives for different elevator positions; Elevator effectivness derivative. Comparison between DUST simulations and Wind Tunnel Testing (Ref. 1)

In Figure 7, the integral loads on the different components of the aircraft in the full configuration are presented, and they are compared with the loads on the horizontal stabilizer in the isolated configuration. Figure 7 (a) shows the vertical force coefficient in body axes as a function of the angle of attack. It is trivial to note that the major component of the aircraft's integral load is given by the load on the wing-pylon system, while a limited part of the load is given by the tail, and consequently, the effect of the wing's downwash is almost negligible for this curve. A similar conclusion can be drawn from the graph in Figure 7 (b) which represents the longitudinal force coefficient as a function of the angle of attack for the various components. In Figure 7 (c), the integral moment coefficient of the aircraft with respect to its center of mass is shown. It can be noted that this time the contribution given by the tail is predominant, and it is stabilizing ($C_{m,CG_{\alpha_{tail}}} < 0$) unlike the wing contribution which is more limited and destabilizing ($C_{m,CG_{\alpha_{wing}}} > 0$). The predominant tail contribution

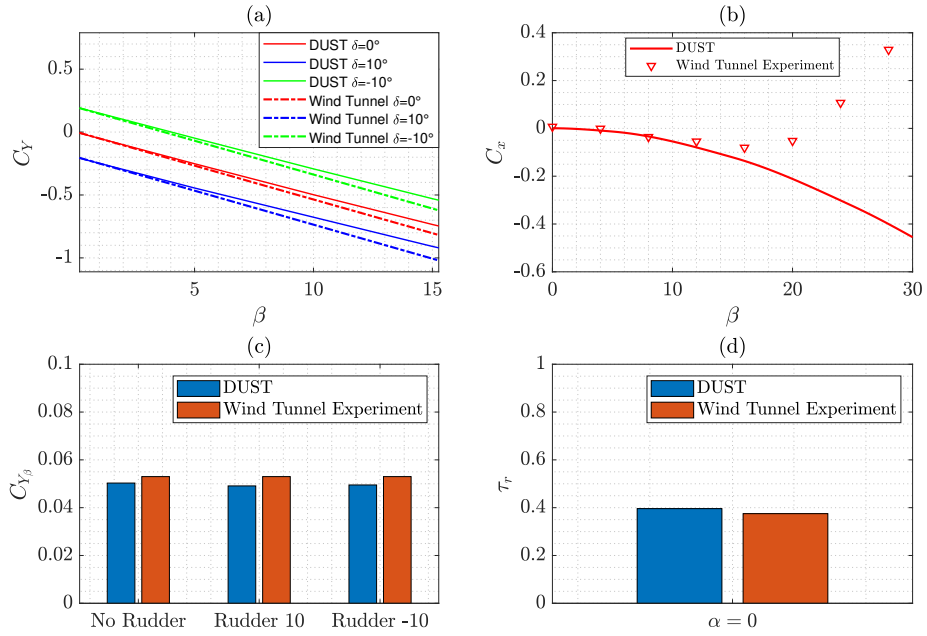

Figure 6. Isolated tail static loads: aerodynamic coefficients as function of the angle of sideslip. unction of the angle of attack; Lateral stability derivatives for different rudder positions; Rudder effectivness derivative. Comparison between DUST simulations and Wind Tunnel Testing (Ref. 1)

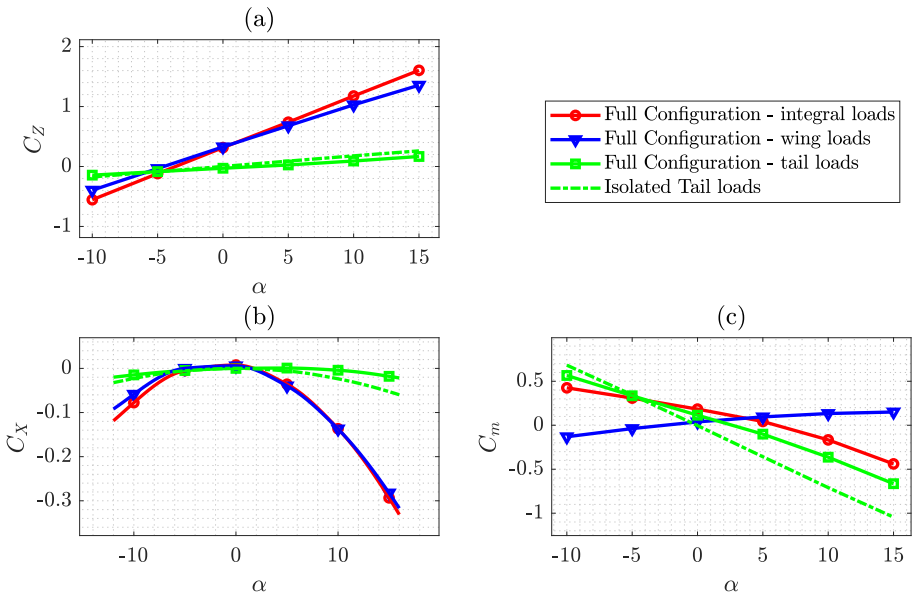

Figure 7. Full configuration breakdown analysis and comparison with the isolated tail load for the longitudinal integral loads coefficients.

leads to the aircraft being overall statically stable in the longitudinal plane ($C_{m,CG_{\alpha_{tot}}} < 0$). It is also important to underline the difference in the moment contribution between the tail in the complete configuration and the isolated tail: the effect of the wing's downwash on the tail this time is not negligible and leads to a decrease in load of about 40%. This highlights the necessity to correctly predict the wing's aerodynamic interaction effect on the tail to adequately predict the aircraft's stability characteristics. In this context, DUST performs well, as also validated by the graph in Figure 8(b) which represents the effect of the induced angle of attack by the wing on the tail for different angles of attack, compared with the wind tunnel data

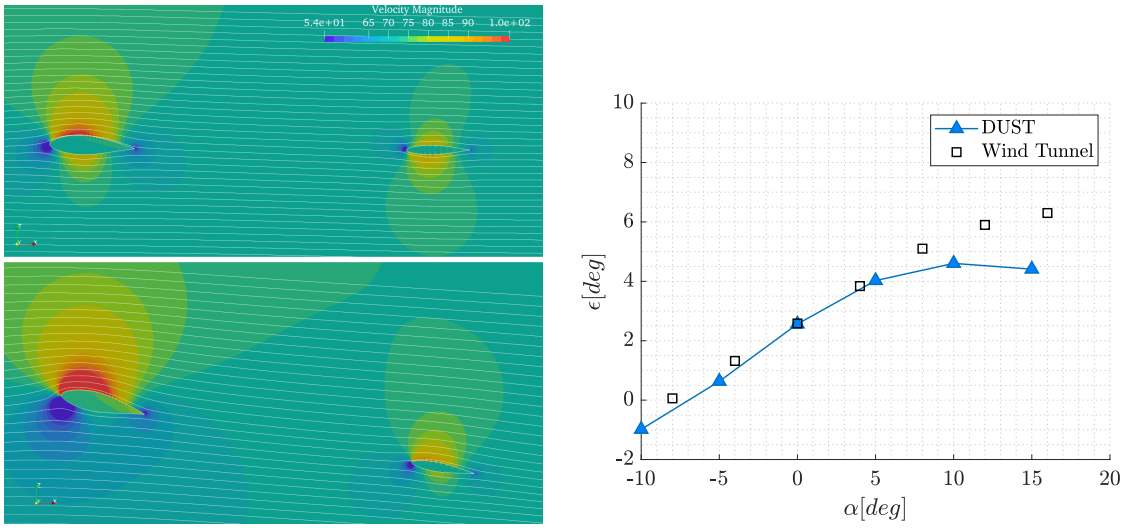

Figure 8. (a) DUST computed flowfield for $\alpha = 0°$ and $\alpha = 10°$ (b) downwash angle as a function of the angle of attack, comparison with wind tunnel experiment from (Ref. 1)

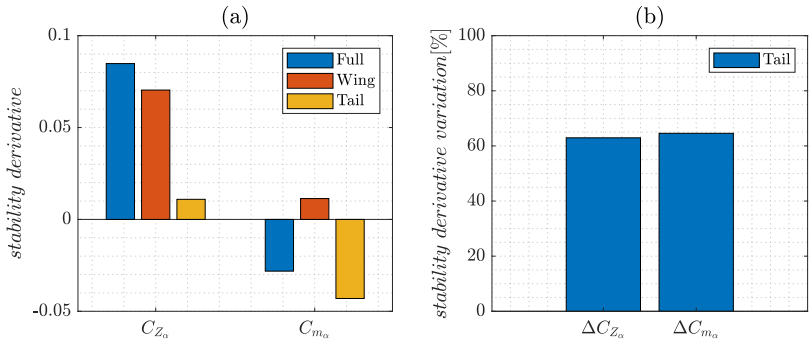

Figure 9. (a) Full configuration without rotors static stability derivatives; (b) percentage variation of the tail static stability derivatives due to the downwash effect

reported in (Ref. 1), and with the same definition of downwash angle ε presented in (Ref. 1). Figure 8(a) instead shows a visualization the flow field influenced by the presence of the main wing on the tail plane, leading to a higher downwash at more pronounced angles of attack.

Figure 9 (a) represents the stability derivatives for each component in the complete configuration, and Figure 9 (b) shows the percentage variation of the tail's stability derivatives due to the downwash effect.

Full Configuration with Rotors

In this section, results associated with the full configuration with rotors are presented. Specifically, the results will be compared with those of the full configuration without rotors, presented in section , to highlight the effects of the rotors on the static stability characteristics of the aircraft in its complete configuration. The geometric parameters of the rotor, such as collective, longitudinal cyclic, and lateral cyclic, were selected in order to match the trim condition described in table 2 and 3, which is associated with an angle of attack of 6.94° and a null sideslip angle. Consequently, these static simulations, which vary angle of attack and sideslip angle, are to be intended as a deviation/perturbation from the trim condition, which on the other hand represents the meaning of stability derivatives in the study of flight mechanics, which are a linear approximation around an equilibrium condition.

In Figure 10, the rotor loads corresponding to the trim condition in the full configuration and with the isolated rotor are visible. The loads are well matched considering that only two parameters were controlled and the discrepancies can be attributed to the interaction between the wing and rotor, which Ferguson (Ref. 1) does not account for in the model.

Table 2. Flight condition parameters (Ref. 1)

Air density	1.225	kg/m^3
Speed	72.022	m/s

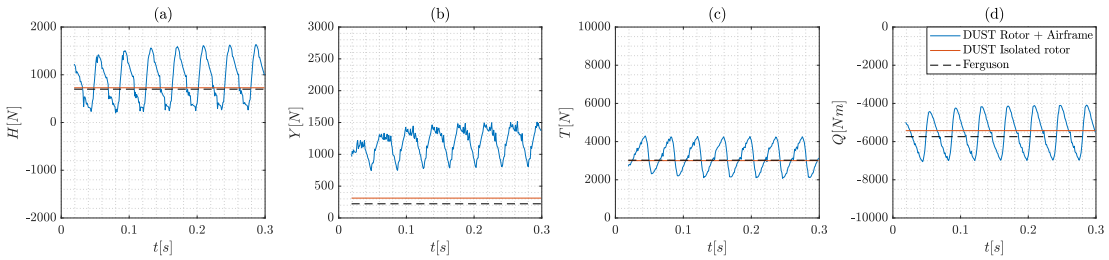

Figure 10. Rotor Loads in the trimmed condition, full configuration, comparison with (Ref. 1)

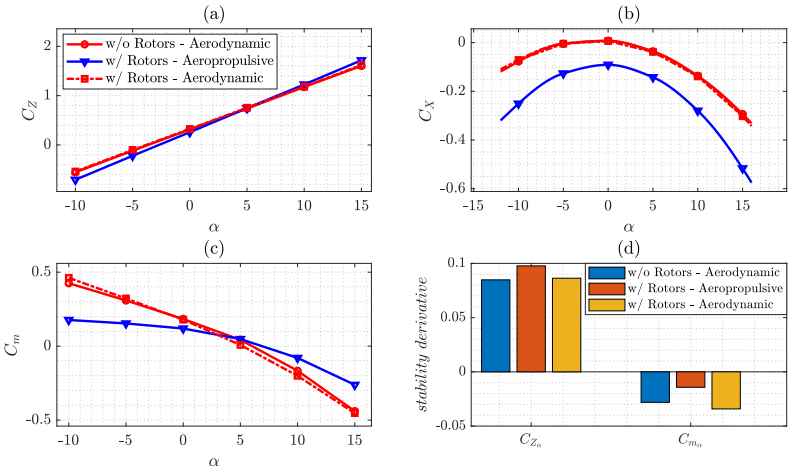

Figure 11. Full configuration with rotors: comparison between aerodynamic and aeropropulsive loads and longitudinal stability derivatives

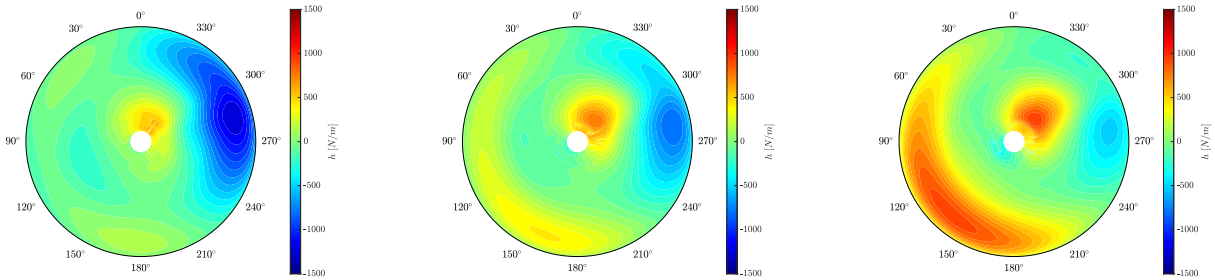

Figure 12. Sectional H-Force acting on the rotor as a function of the azimuthal angle (a) $\alpha = 0°$ (b) $\alpha = 5°$ (c) $\alpha = 10°$

In Figure 11, the comparison between the vertical force, longitudinal force, and pitching moment coefficients of the full configuration with rotors is shown, distinguishing the forces of the airframe (pure aerodynamic forces), the aeropropulsive forces (airframe and rotors) and compared with the airframe forces in the full configuration without rotors. It is noticeable on the $C_Z - \alpha$ graph an increase in slope for the aeropropulsive forces curve, while the airframe forces remained almost unchanged. Consequently, the variation in the case of aeropropulsive forces can be attributed to the rotor loads alone and not to the wing-rotor interaction. The same comment applies to the $C_X - \alpha$ graph, where the shift of the aeropropulsive forces is associated with the thrust of the rotor (positive towards the tail of the aircraft, therefore a downward shift). The same conclusion also applies to the pitching moment, where, however, the increase in slope is due to an increase towards a positive value of C_{m_α} (thus destabilizing). This leads to a consequent variation of the static stability derivatives of the complete aircraft (Fig. 11 (d)). The behavior of the curves can be justified by studying the H-force on the rotor as a function of the angle of attack: from Figure 12, it can be noted that the tendency of the H-force is to become increasingly positive

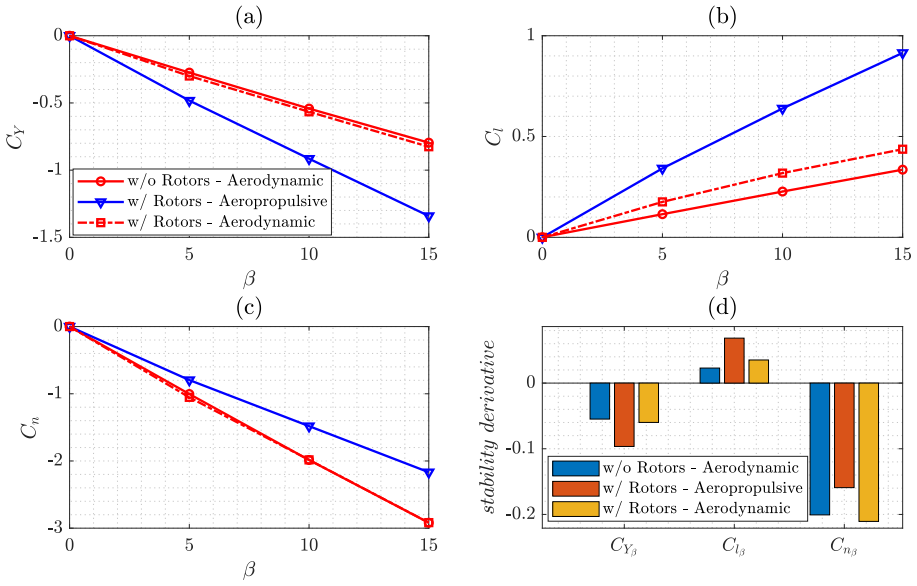

Figure 13. Full configuration with rotors: comparison between aerodynamic and aeropropulsive loads and lateral stability derivatives

Table 3. Trim parameters (Ref. 1)

Mode	Airplane	[um]
Pitch Angle	6.944	deg
Rotor Speed	517	RPM
Rotor Collective	29.5015	deg
Elevator	-1.2398	deg

as the angle of attack increases and this justifies the increase in the derivative C_{Z_α}. Moreover, since the rotors are positioned in front of the CG of the aircraft, the increase in C_Z is translated into a positive increase in pitching moment, hence a destabilizing contribution.

The same behavior can be seen in figure 13, where the sideslip angle is varied, and this leads to an increase in the stability derivatives C_{Y_β} and C_{l_β}, and a decrease in the magnitude of the stability derivative C_{n_β}.

It is important to emphasize that this is a physical behavior that is expected on the full configuration with rotors, but the most relevant aspect is that DUST allows for precise quantification of the rotor's contribution to stability derivatives, which is the real added value compared to more classical methods of determining the static and dynamic stability properties of aircraft.

DYNAMIC ANALYSES

In this chapter, the results obtained from dynamic simulations for the various configurations tested will be presented. The study focuses on stability derivatives relative to a roll rate p, hence calculating C_{Y_p}, C_{l_p}, and C_{n_p} for the various configurations. The methodology used for calculating the dynamic

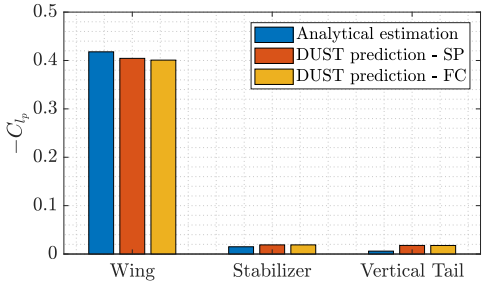

Figure 14. Validation of the aerodynamic numerical methodology of calculation of dynamic stability derivatives. (Ref. 11)

stability derivatives was presented in the previous section. The dynamic motion is simulated using DUST software and a time-marching simulation. The rolling motion is executed around the trim condition presented in the previous chapter, maintaining the same flight conditions.

Figure 14 illustrates the validation of the calculation method (under the previously mentioned trim conditions) for the C_{l_p} stability derivative for the individual components of the aircraft. The stability derivatives obtained with the dynamic simulations carried out using DUST show excellent correspondence with the analytical method presented in reference (Ref. 11), thus demonstrating the suitability of the model built on DUST for calculating dynamic stability derivatives.

Full Configuration without Rotors

In this section, the results obtained from the dynamic simulations on the XV-15 are once again compared using a breakdown approach. The simulated motion is a dynamic rolling

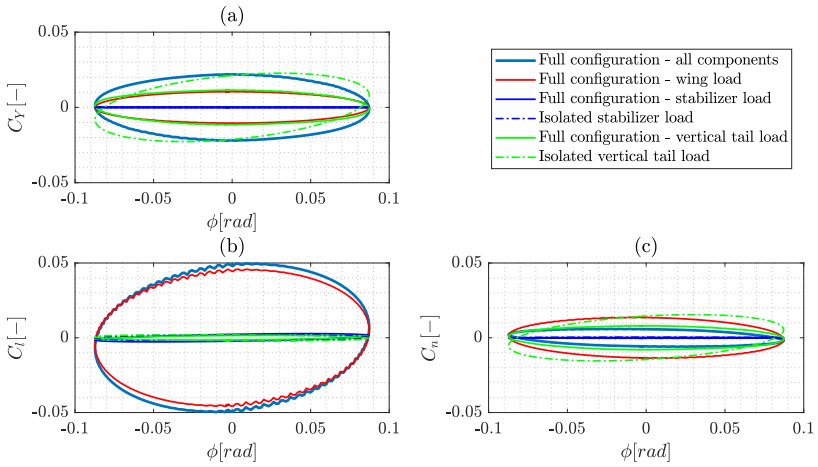

Figure 15. Rolling oscillation: Aerodynamic coefficients as function of the Roll angle.

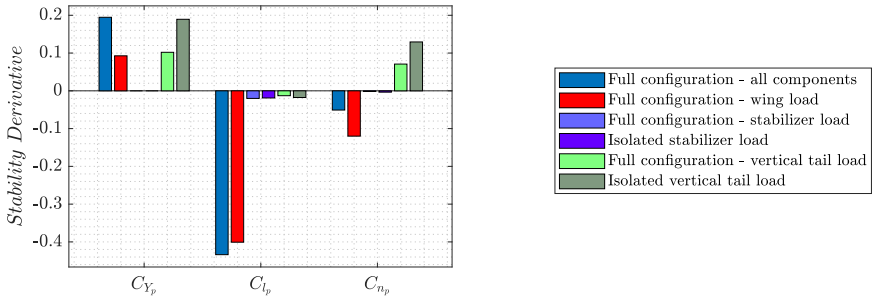

Figure 16. Rolling oscillation: Dynamic Stability Derivatives computed with the Fourier Coefficient Method

oscillation around the trim condition outlined in table 2, at a frequency of 3 Hz for 1 second of simulation. The amplitude of oscillation is 5° in roll, with the angle of attack corresponding to the trim condition. Only the last period of oscillation is shown, where the solution has reached a periodic steady-state condition after an initial transient. The lateral force, roll moment , and yaw moment coefficients are plotted against the roll angle ϕ, and since the context is of linear aerodynamics, the sinusoidal motion translates in this graph into a hysteresis ellipse that describes the load path over time, as clearly visible in figure 15.

If the ellipse is traversed clockwise, the dynamic stability derivative will be positive, and in the opposite case, where the ellipse is traversed counterclockwise, the derivative will be negative.

In Figure 15, the time histories during the oscillatory roll motion of the different components are shown, both in the full configuration and in the isolated configuration. The term "isolated vertical load" refers to the load on the vertical tail in the tail-only configuration (thus including the horizontal stabilizer), while "isolated stabilizer load" denotes the load on the horizontal stabilizer in the tail-only configuration.

In Figure 15 (a), it can be observed that for the lateral force coefficient C_{Y_p}, the most significant contribution logically comes from the vertical tail, while the horizontal stabilizer has practically no contribution. Furthermore, by comparing with the isolated load, it is evident that the hysteresis (and therefore the derivative C_{Y_p}) is influenced by the downwash effect of the wing on the tail. A similar observation can be made for the yaw moment coefficient C_{n_p} graph in Fig. 15 (c).

The roll moment coefficient graph assumes a particularly significant physical meaning: it describes how the aerodynamic roll moment acts in response to a roll motion. From a physical standpoint, aerodynamic forces tend to dampen motions occurring in a fluid, and indeed, the hysteresis curve in Fig 15 (b) is an ellipse that runs counterclockwise for all components: the aerodynamic moment tends to counteract the motion that the aerodynamic surfaces are undergoing. The aerodynamic damping is proportional to the size of the component (in fact, almost the entire ellipse is due to the contribution of the wing), and the effect of downwash does not influence the aerodynamic damping.

In Figure 16, the dynamic stability derivatives are extracted from the hysteresis curves of Figure 15 using the Single Point and Fourier Coefficient methods. particularly relevant are the derivatives of the component C_{l_p}, also known as the "damping in roll derivative," whose value is proportional to the aerodynamic damping of the component. It can also be seen that the tail derivatives are influenced by the downwash effect.

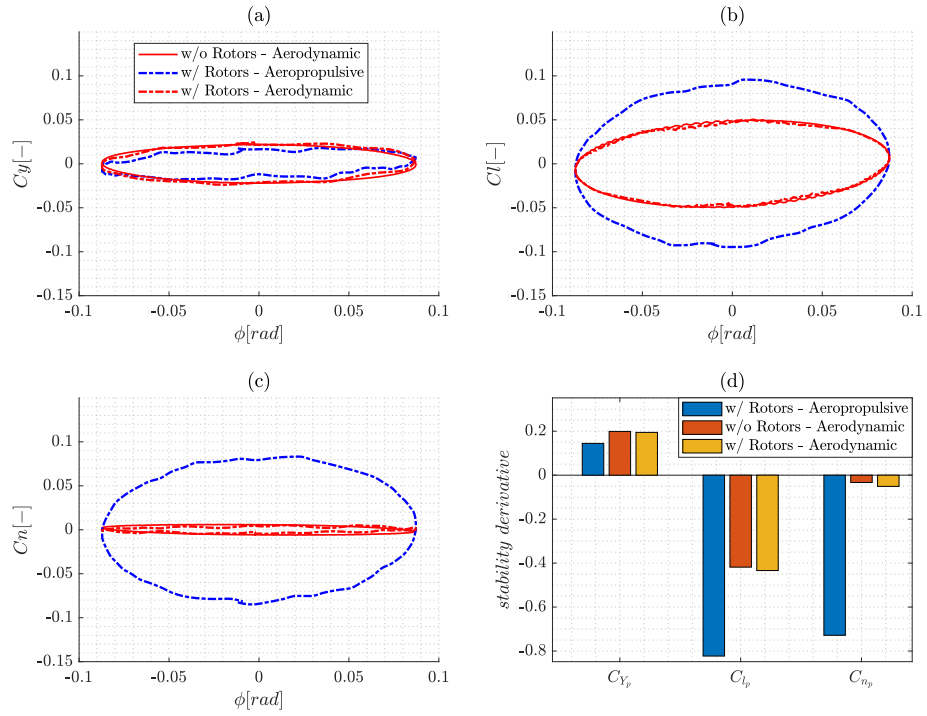

Figure 17. Rolling oscillation: Aerodynamic coefficients as function of the Roll angle and Dynamic Stability Derivatives.

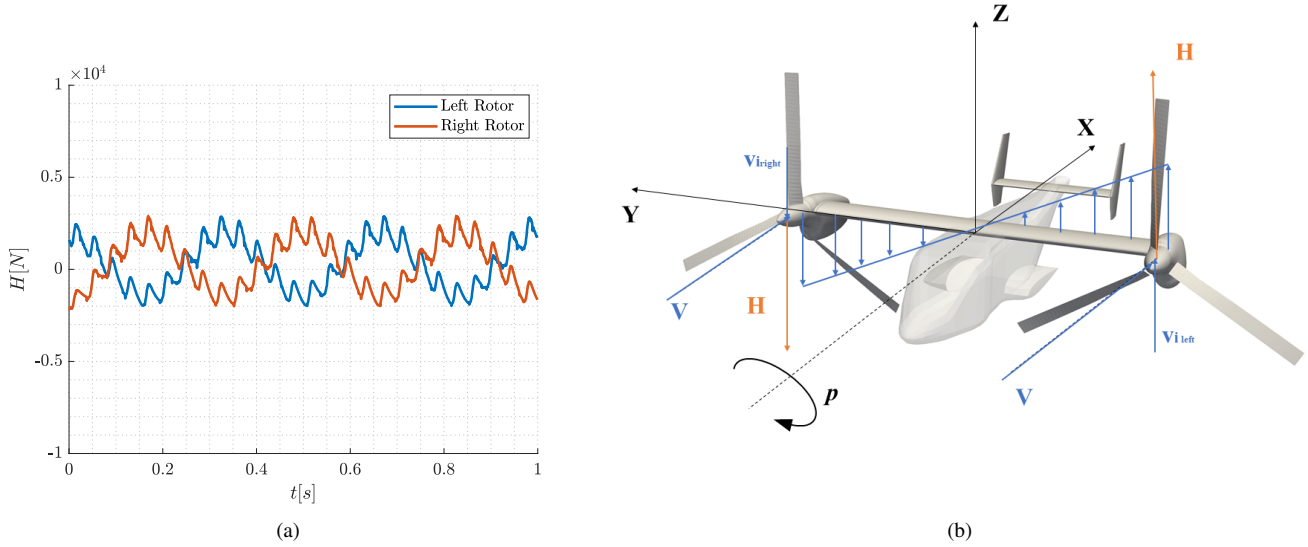

Figure 18. (a) H-Force acting on the rotors as a function of time (b) graphical representation of the forces acting on the aircraft.

Full Configuration with Rotors

In this section, the aerodynamic and aeropropulsive loads obtained from dynamic tests with the rotor are compared with those obtained without rotor, to highlight the influence of the rotor on the stability derivatives and more generally on the stability characteristics of an aircraft.

Figure 17 shows the temporal history of aerodynamic and aeropropulsive loads, which describe hysteresis curves. It can be noted that, similarly to the static case, the wing-rotor interaction has a limited influence on the airframe load in the context of stability derivatives evaluation. However, when considering the aeropropulsive curves, significant changes start to be noticeable: in particular, the highly oscillating load on

the rotor leads to a periodic irregularity on the ellipse, resulting in its deformation. This irregularity does not affect the calculation of the derivatives, as it is considered as a higher harmonic added to the Taylor expansion described in chapter . Nevertheless, the absolute load on the rotor leads to non-negligible variations in the stability properties: it is observed that the hysteresis curves of the C_l and C_n moments are enlarged, leading to a significant change in the dynamic stability derivative (Fig. 17 (d)). In particular, the roll damping derivative C_{l_p} is increased, meaning the rotor's effect is damping on the overall behavior of the aircraft and tends to counteract the rolling motion.

This behavior is justifiable from a physical standpoint: assuming a positive roll motion, there is an induced velocity distribution from the motion as represented in figure 18(b). Consequently, there is a positive change in H-force towards the positive z-axis for the left rotor and a negative change for the right rotor. This pair of forces creates a moment that counters the rolling motion, thereby increasing the overall damping properties of the aircraft. This phenomenon highlights the importance of the rotor in determining the stability and control properties of an aircraft, especially in configurations with multiple rotors or hybrid configurations.

Figure 18(a) displays the temporal history of the H-force, which behaves in an equal and opposite manner on the two rotors, thereby generating a torque that opposes and damps the motion, hence increasing the stability derivatives.

CONCLUSIONS

The present activity was aimed to investigate the potentiality of the use of a mid-fidelity aerodynamic software for the calculation of the static and dynamic stability derivatives of a tiltrotor aircraft. With this aim, the well known Bell XV-15 was used as a test case, thanks to the availability in literature of a comprehensive experimental data base for the evaluation of stability derivatives of this aircraft. Simulations with the mid-fidelity solver DUST were performed to evaluate the aircraft aerodynamic coefficients for both static attitudes and harmonic motions of the aircraft and their outcomes were used to compute respectively static and dynamic stability derivatives by using two different mathematical methods.

Results obtained using the mid-fidelity numerical approach showed a quite good agreement with experimental data and provide also a similar level of accuracy with respect to the stability derivative values calculated with high-fidelity CFD approach available in literature. A limit of the mid-fidelity approach was found considering conditions with the occurrence of consistent flow separation that could not be accurately reproduced by panel methods.

Nevertheless, the quite low computational effort required by this approach and the quite good accuracy obtained with respect to both experiments and high-fidelity CFD opens a new scenario for the evaluation of rotorcraft stability derivatives.

Also, these simulations provided valuable design considerations for tiltrotor aircrafts, such as the quantification of the effect of downwash and the rotor's influence on stability derivatives. These findings have important implications for the design and development of such an innovative configuration, and they demonstrate the effectiveness of the mid-fidelity approach in providing valuable insights into the aircraft's behavior and performance in different flight conditions.

REFERENCES

1. Ferguson, S. W., "A mathematical model for real time flight simulation of a generic tilt-rotor aircraft," *NASA CR-166536*, Vol. 1, 1988.

2. Loeser, T. D., Schuette, A., *et al.*, "SACCON Forced Oscillation Tests at DNW-NWB and NASA Langley 14x22-foot Tunnel," Technical report, 2010.

3. Bergmann, A., Huebner, A., and Loeser, T., "Experimental and numerical research on the aerodynamics of unsteady moving aircraft," *Progress in Aerospace Sciences*, Vol. 44, (2), 2008, pp. 121–137.

4. Ventura Diaz, P., and Yoon, S., "Computational study of NASA'S quadrotor urban air taxi concept," AIAA SciTech 2020 Forum, 2020.

5. Tugnoli, M., Montagnani, D., Syal, M., Droandi, G., and Zanotti, A., "Mid-fidelity approach to aerodynamic simulations of unconventional VTOL aircraft configurations," *Aerospace Science and Technology*, Vol. 115, 2021, pp. 106804.

6. Granata, D., Savino, A., and Zanotti, A., "Numerical Evaluation of Aircraft Aerodynamic Static and Dynamic Stability Derivatives by a Mid-Fidelity Approach," *Aerospace*, Vol. 11, (3), 2024, pp. 213.

7. Ronch, A. D., Vallespin, D., Ghoreyshi, M., and Badcock, K., "Evaluation of dynamic derivatives using computational fluid dynamics," *AIAA journal*, Vol. 50, (2), 2012, pp. 470–484.

8. Savino, A., Cocco, A., Zanotti, A., Tugnoli, M., Masarati, P., and Muscarello, V., "Coupling mid-fidelity aerodynamics and multibody dynamics for the aeroelastic analysis of rotary-wing vehicles," *Energies*, Vol. 14, (21), 2021, pp. 6979.

9. Tran, S. A., and Lim, J. W., "Interactional Aerodynamics of the XV-15 Tiltrotor Aircraft during Conversion Maneuvers," *Journal of the American Helicopter Society*, Vol. 67, (3), 2022, pp. 56–68.

10. Savino, A., "A Mid-Fidelity Aeroelastic Environment for Tiltrotor Analysis and Design," , 2022.

11. Finck, R., "USAF (United States Air Force) Stability and Control DATCOM (Data Compendium)," *Defense Technical Information Center*, 1978.